

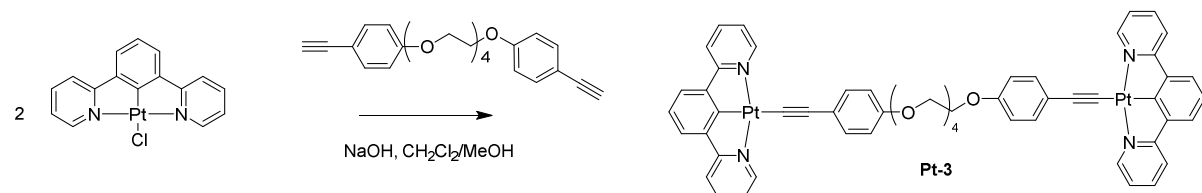
Controlling the Emission in Flexibly-Linked (N^C^N)Platinum Dyads

Eleonora Garoni,^[a,b] Julien Boixel,^[a] Vincent Dorcet,^[a] Thierry Roisnel,^[a] Dominique Roberto,^[b] Denis Jacquemin,^{*[c,d]} and Véronique Guerchais^{*[a]}

Electronic Supporting Information

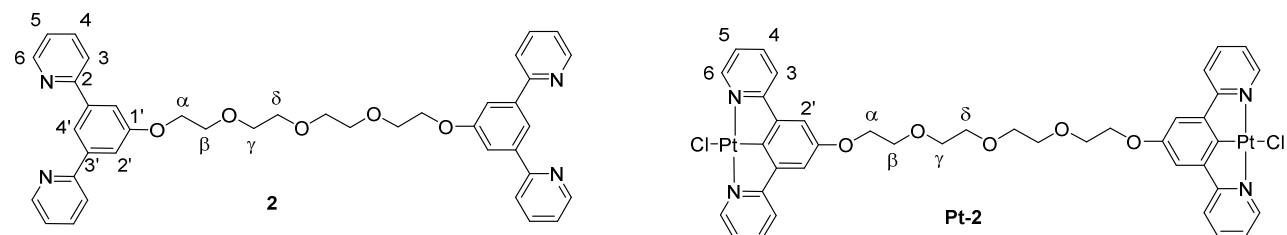
Table of contents :

Characterization of precursors and complexes.....	S2
X-ray crystal structure determination.....	S7
Additional Photophysical spectra.....	S10
Additional theoretical results.....	S15
References:	S18



Scheme S1. Synthesis of complex **Pt-3**.

Numbering



Characterization of precursors and complexes

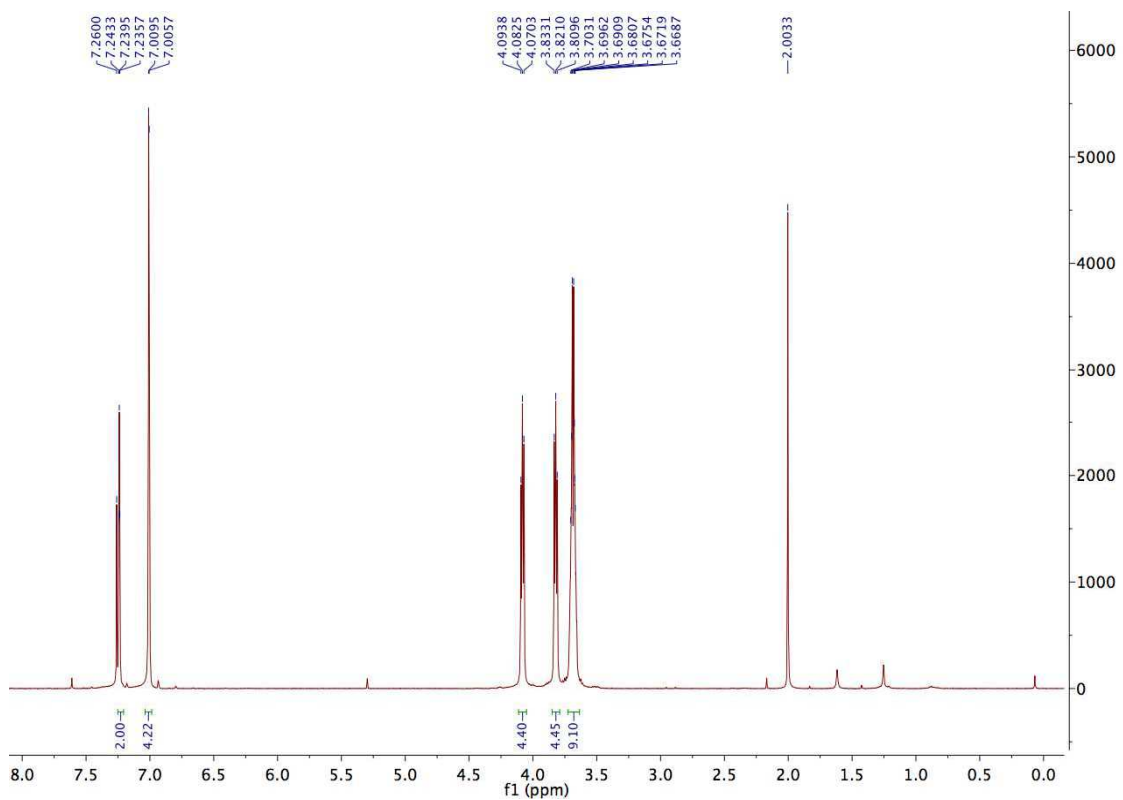


Figure S1. ^1H NMR spectrum of **1** in CDCl_3 .

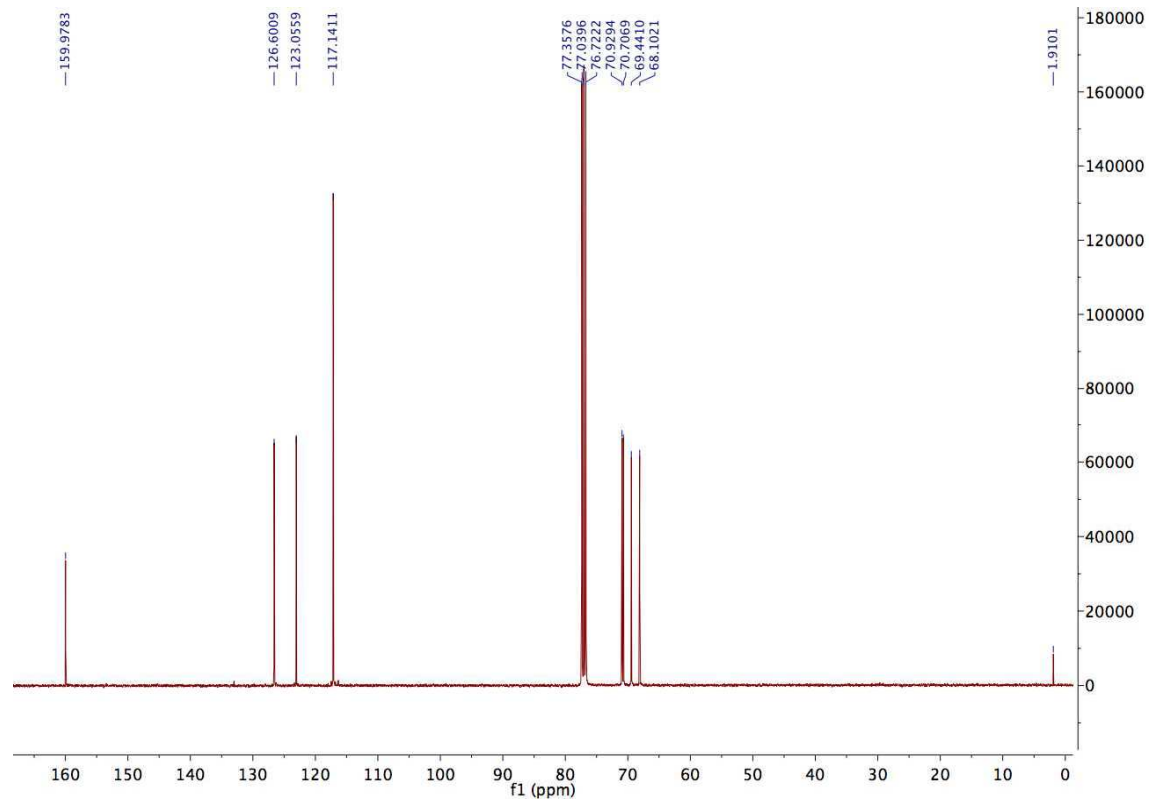


Figure S2. ^{13}C NMR spectrum of **1** in CDCl_3 .

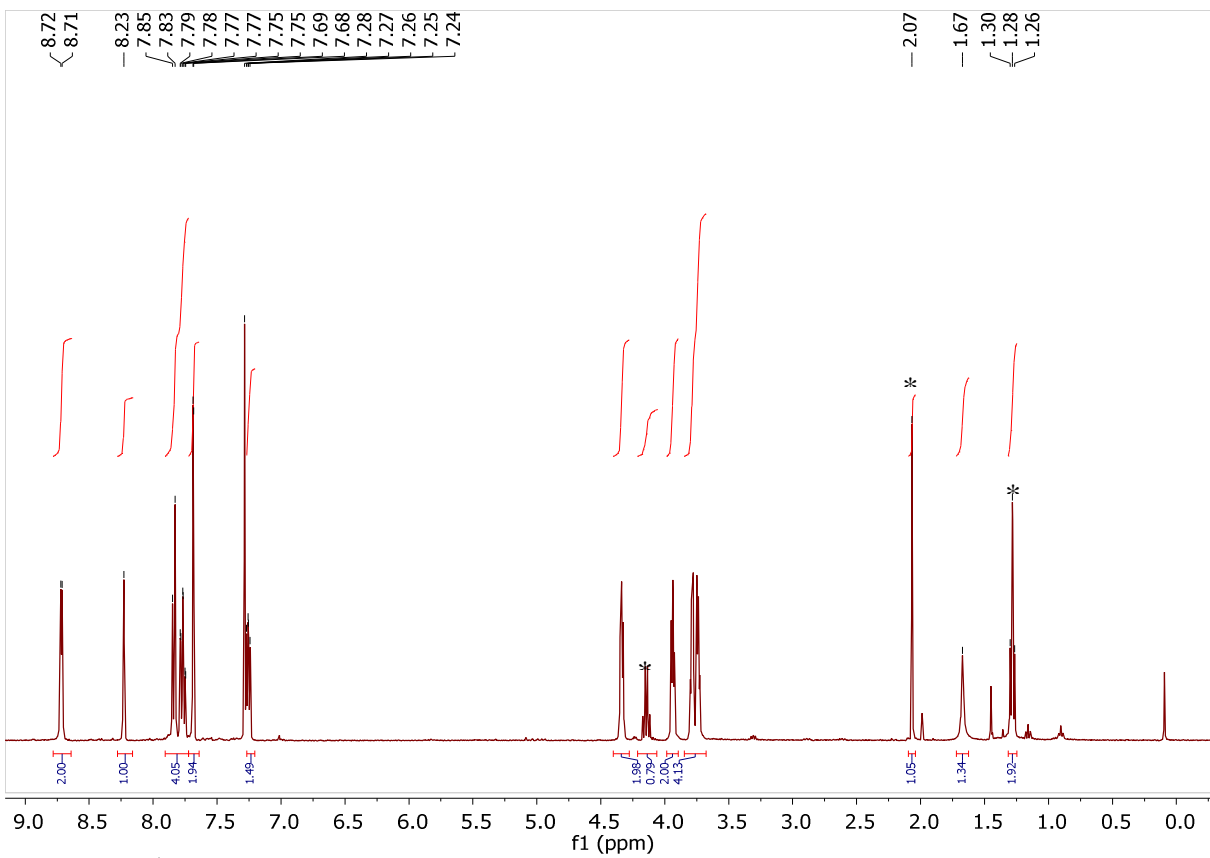


Figure S3. ^1H NMR spectrum of **2** in CDCl_3 . *AcOEt.

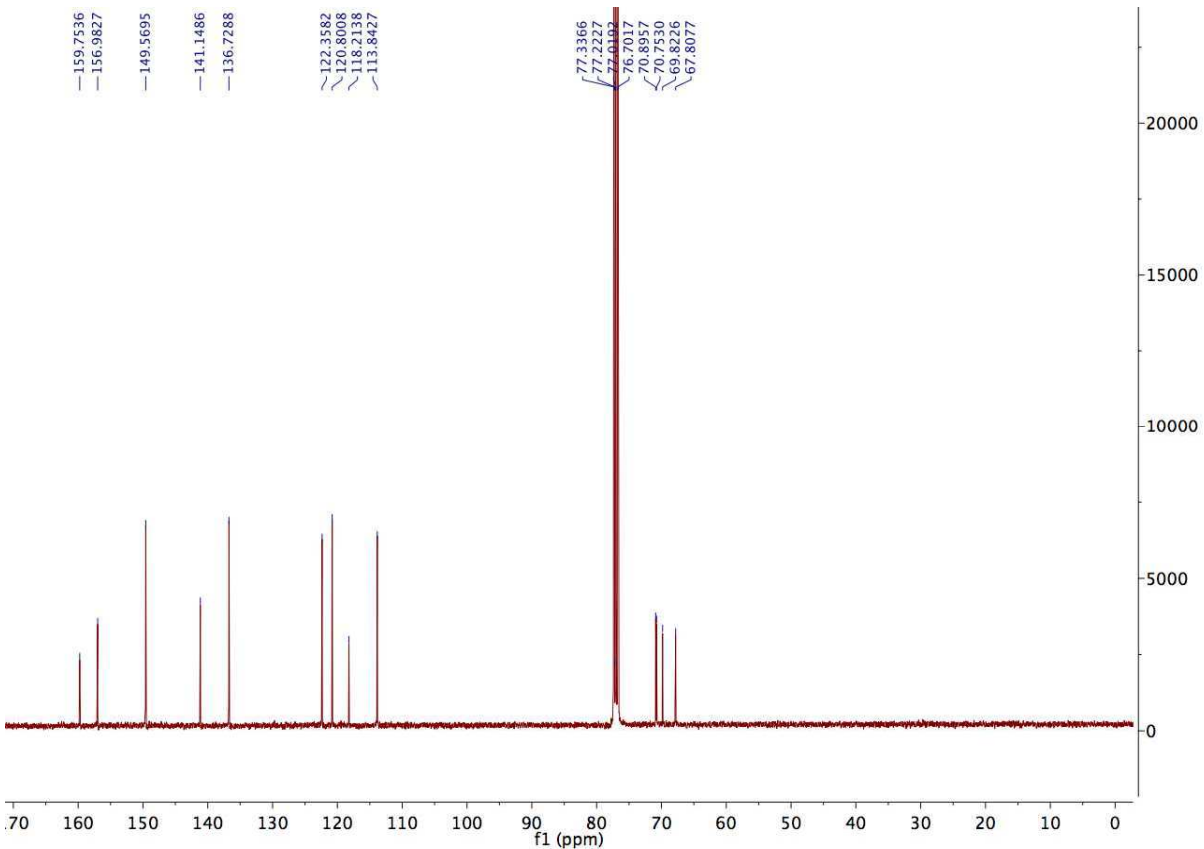


Figure S4. ^{13}C NMR spectrum of **2** in CDCl_3 .

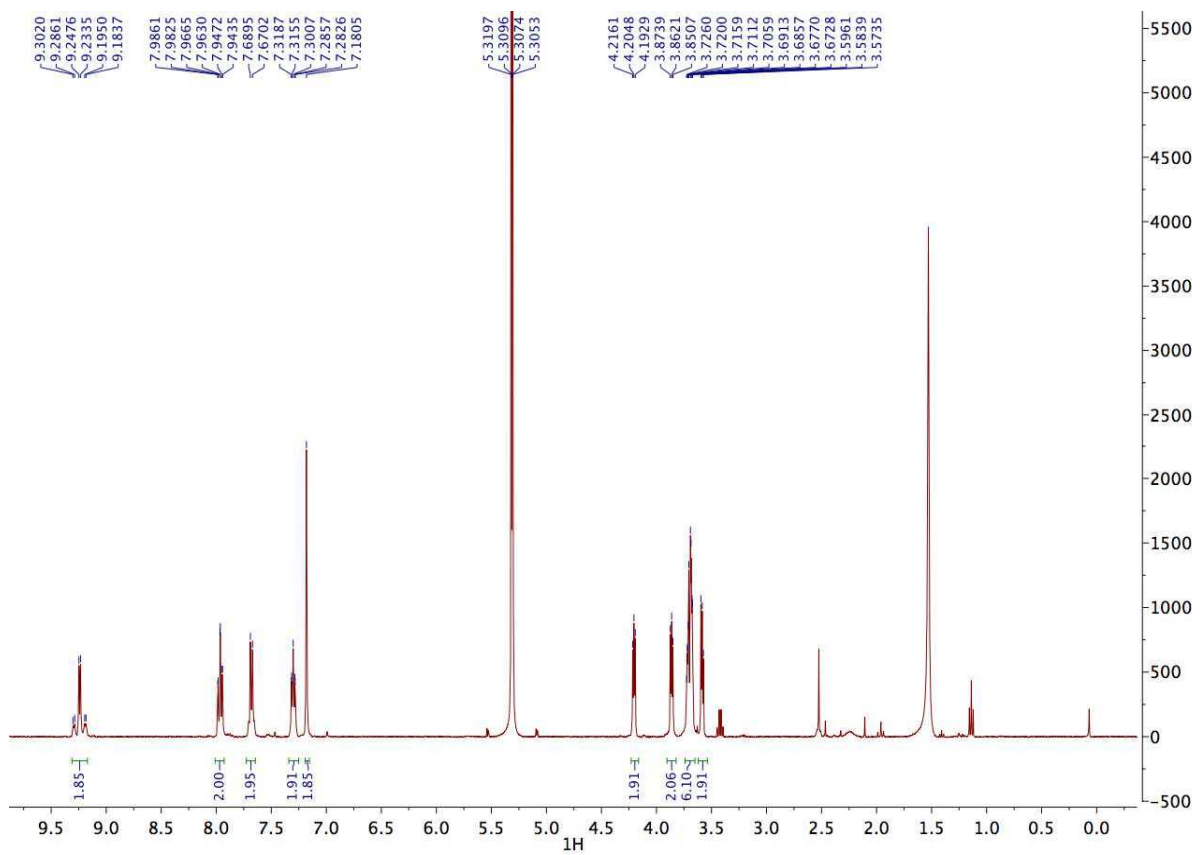


Figure S5. ^1H NMR spectrum of **Pt-1** in CD_2Cl_2 .

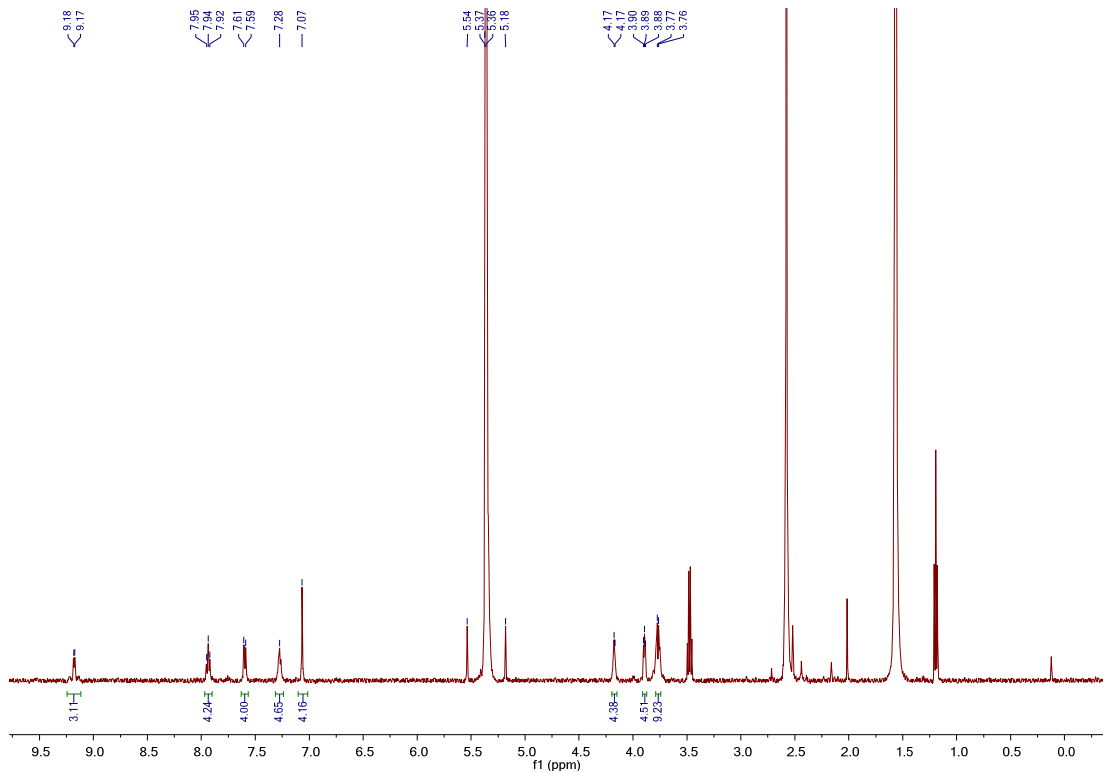


Figure S6. ^1H NMR spectrum of **Pt-2** in CD_2Cl_2 .

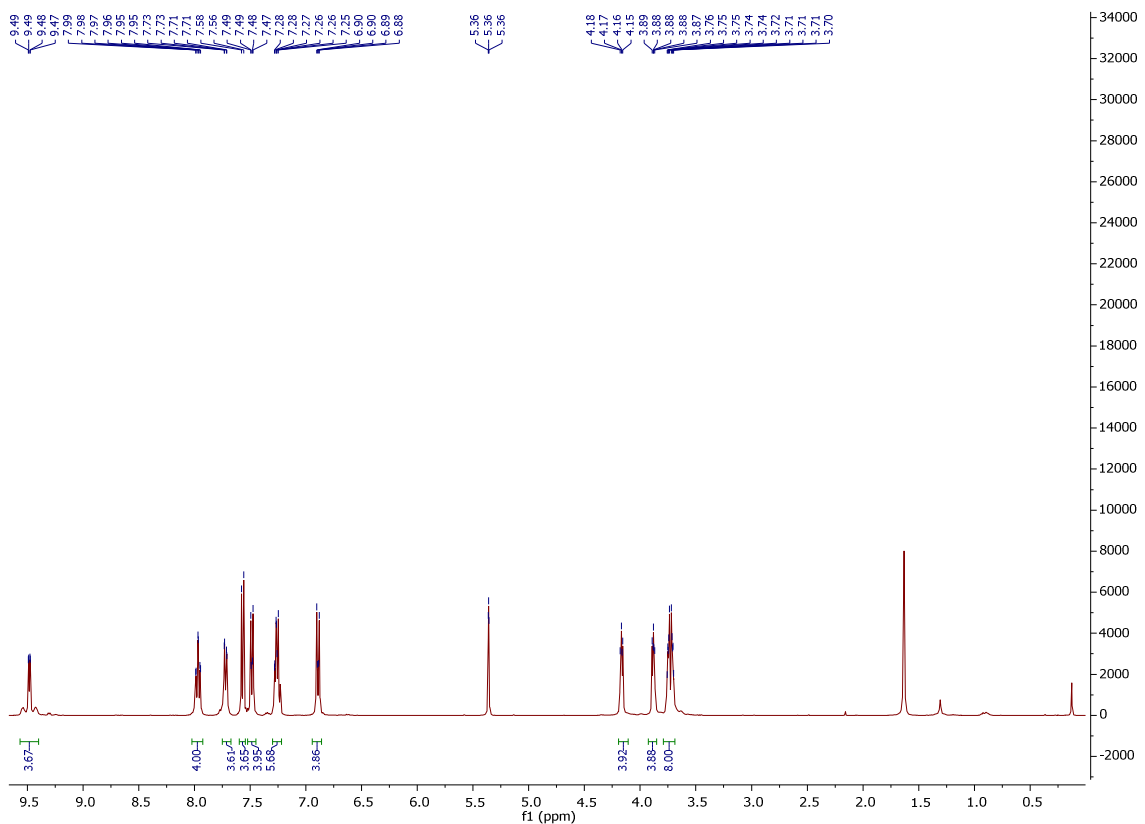


Figure S7. ^1H NMR spectrum of Pt-3 in CD_2Cl_2 .

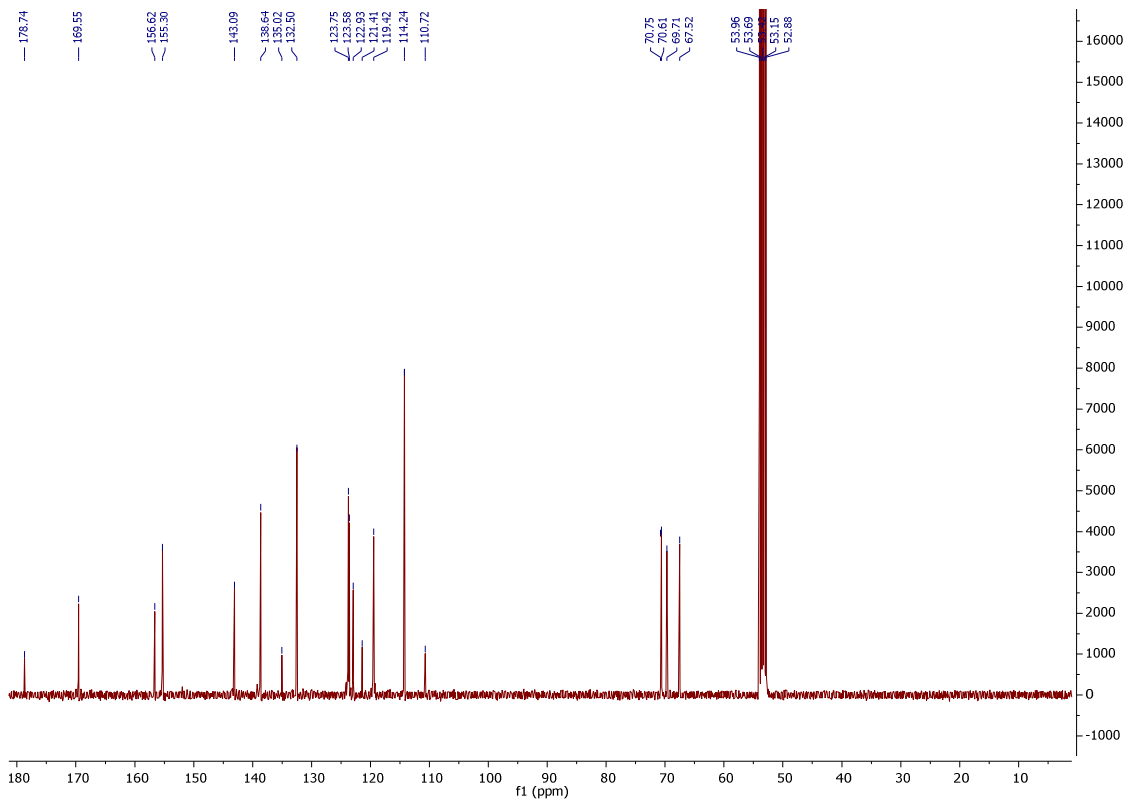


Figure S8. ^{13}C NMR spectrum of Pt-3 in CD_2Cl_2 .

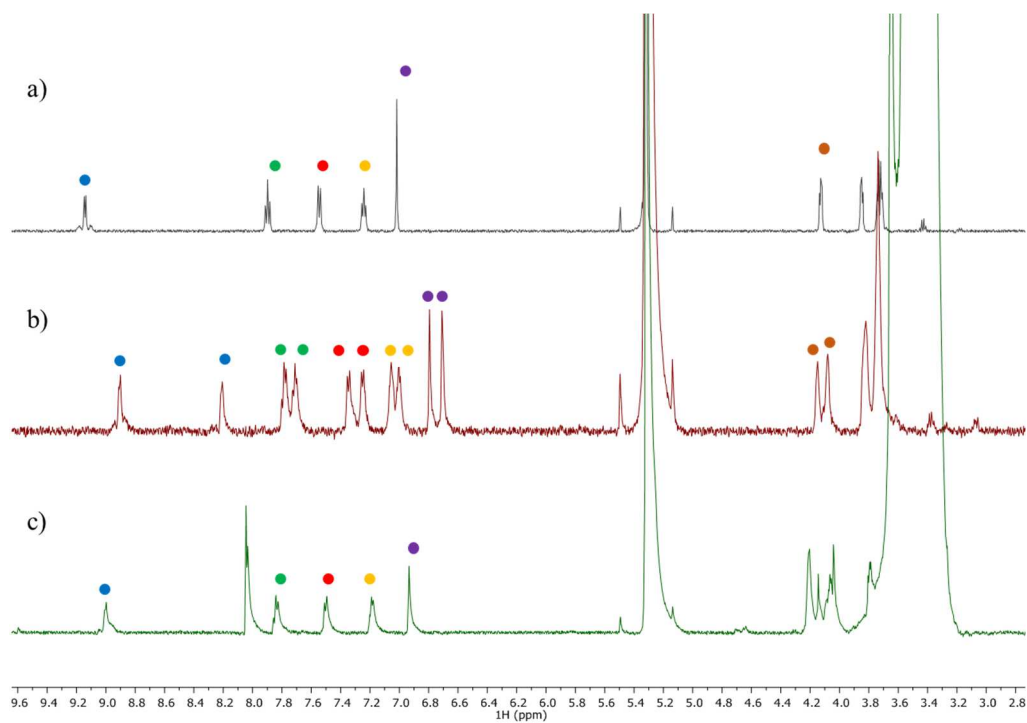


Figure S9. ^1H NMR spectra of (a) **Pt-2** in CD_2Cl_2 , (b) after addition of 10 equiv. of KPF_6 in CD_3CN , (c) after further addition of 20 equiv. of 18-crown-6 in CD_2Cl_2 .

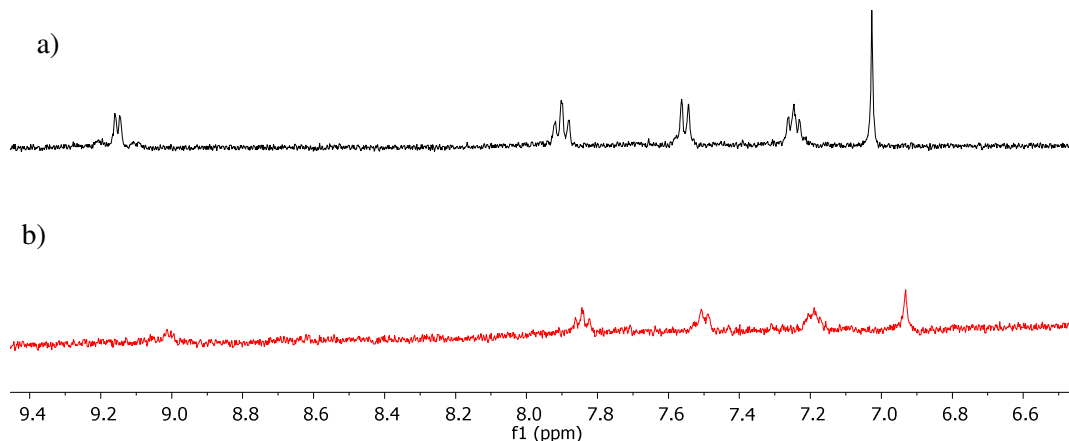


Figure S10. ^1H NMR spectra of **Pt-2** in CD_2Cl_2 (a) before (b) after addition of 10 equiv. of $\text{CH}_3\text{CO}_2\text{Cs}$.

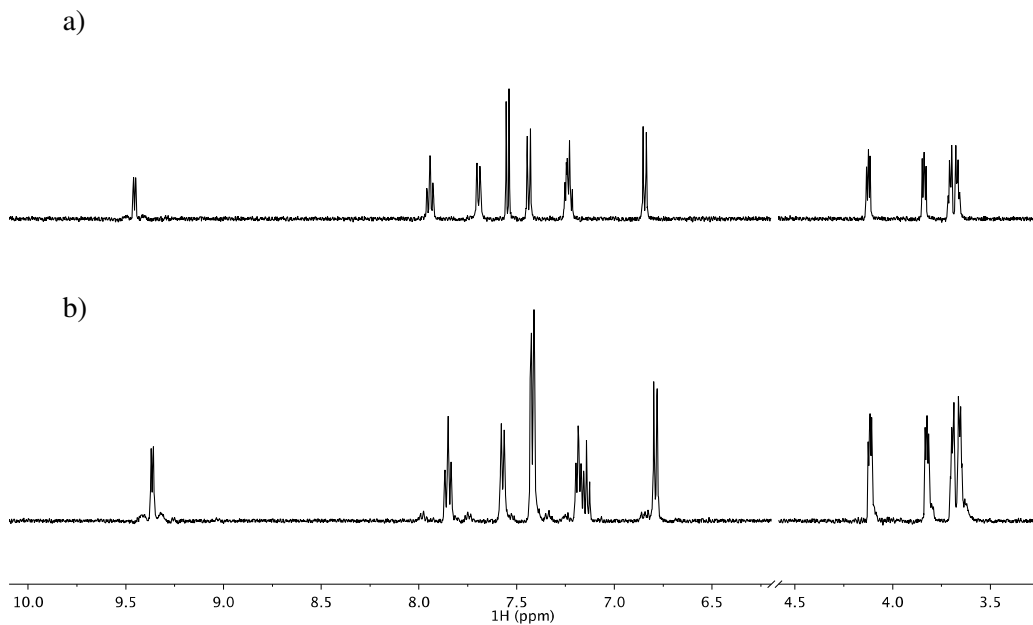
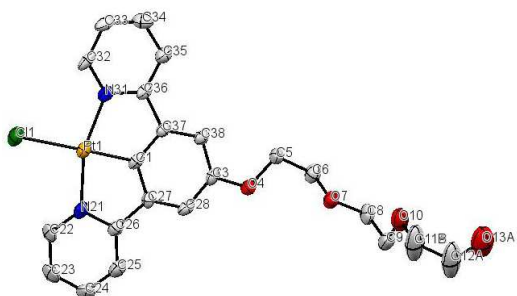


Figure S11. ^1H NMR spectra of (a) **Pt-3** in CD_2Cl_2 , (b) after addition of 10 equiv. of KPF_6 in CD_3CN .

X-ray crystal structure determination

Orange crystals were grown by slow diffusion of diethyl ether into a concentrated dichloromethane solution of **Pt-1**. A crystal of dimensions $0.45 \text{ mm} \times 0.36 \text{ mm} \times 0.1 \text{ mm}$ mounted on a cryoloop was used for data collection. Intensity data were collected at 150 K in a D8 VENTURE Bruker AXS diffractometer. Crystal data for $\text{C}_{22}\text{H}_{22}\text{ClN}_2\text{O}_4\text{Pt}$ ($M = 608.95$): Mo-K α radiation ($\lambda = 0.71073 \text{ \AA}$), $T = 150 \text{ K}$; monoclinic $P\ 2_1/c$ (I.T.#14), $a = 14.7007(18)$, $b = 17.547(2)$, $c = 8.3565(9) \text{ \AA}$, $\beta = 105.283(4)^\circ$, $V = 2079.3(4) \text{ \AA}^3$, $Z = 4$, $d = 1.945 \text{ g.cm}^{-3}$, $\mu = 6.909 \text{ mm}^{-1}$. The structure was solved by direct methods using the *SHELXT* program,¹ and then refined with full-matrix least-square methods based on F^2 (*SHELXL-2014*).² All non-hydrogen atoms were refined with anisotropic atomic displacement parameters. H atoms were finally included in their calculated positions. A final refinement on F^2 with 4760 unique intensities and 271 parameters converged at $\omega R(F^2) = 0.1689$ ($R(F) = 0.0538$) for 3997 observed reflections with $I > 2\sigma(I)$.

CCDC: 1556598 contains the supplementary crystallographic data for this paper. These data are provided free of charge by The Cambridge Crystallographic Data Centre. Table **S1** contains a summary of crystallographic data.



Bond lengths:

Pt1 - C1 = 1.899(8), Pt1 - N31 = 2.041(7), Pt1 - N21 = 2.043(7), Pt1 - Cl1 = 2.417(2), C3 - O4 = 1.357(10)

Bond Angles

C1 - Pt1 - N31 = 81.0(3), C1 - Pt1 - N21 = 80.0(3), N31 - Pt1 - Cl1 = 99.9(2), N21 - Pt1 - Cl1 = 99.2(2), C3 - O4 - C5 = 116.7(7)

Table S1. Crystallographic data for complex Pt-1

Empirical formula	C ₂₂ H ₂₂ ClN ₂ O ₄ Pt
Formula weight	608.95
Temperature	150 K
Wavelength	0.71073 Å
Crystal system	Monoclinic
Space group	P 21/c
a (Å)	14.7007(18)
b (Å)	17.547(2)
c (Å)	8.3565(9)
α (°)	90
β (°)	105.283(4)
γ (°)	90
Volume (Å ³)	2079.3(4)
Z	4
ρ_{calcd} (g cm ⁻³)	1.945
μ (mm ⁻¹)	6.909
F(000)	1180
Crystal size (mm ³)	0.450 x 0.360 x 0.100
Crystal colour	orange
θ range	3.099-27.483
h_min, h_max	-19, 19
k_min, k_max	-21, 22
l_min, l_max	-10, 10
Reflections collected / unique	23629 / 4760 [R(int) ^a = 0.0533]
Reflections [I>2σ]	3997
Completeness to theta_max	0.998
Absorption correction type	multi-scan
Max. and min. transmission	0.501-0.261
Refinement method	Full-matrix least-squares on F^2
Data / restraints / parameters	4760 / 0 / 271
^b Goodness-of-fit	1.504
Final R indices [I>2σ]	$R1^c = 0.0538$, $wR2^d = 0.1689$
R indices (all data)	$R1^c = 0.0643$, $wR2^d = 0.1837$
Largest diff. peak and hole	2.509, -2.731 e ⁻ .Å ⁻³

Additional Photophysical spectra.

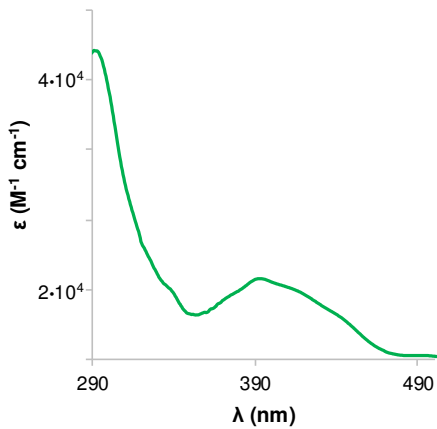


Figure S12. UV-vis. absorption spectrum of **Pt-3** in CH_2Cl_2 solution.

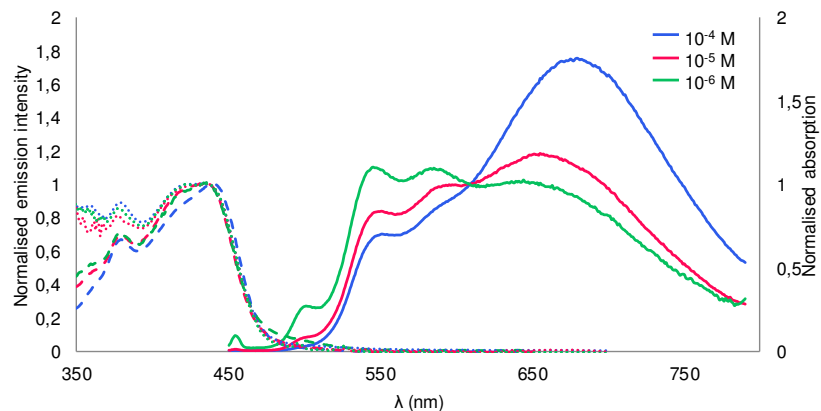


Figure S13. Absorption (dotted lines), emission (plain lines) and excitation (dashed lines) spectra of **Pt-2** in CH_2Cl_2 at different concentrations.

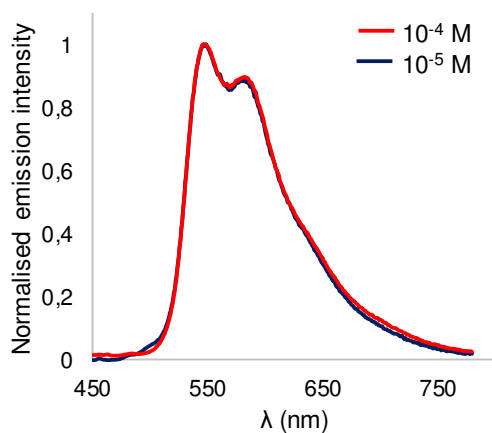


Figure S14. Emission spectra ($\lambda_{\text{exc}} = 400$ nm) of **Pt-1** in CH_2Cl_2 (10^{-4} M, red line) and 10^{-5} M (blue line).

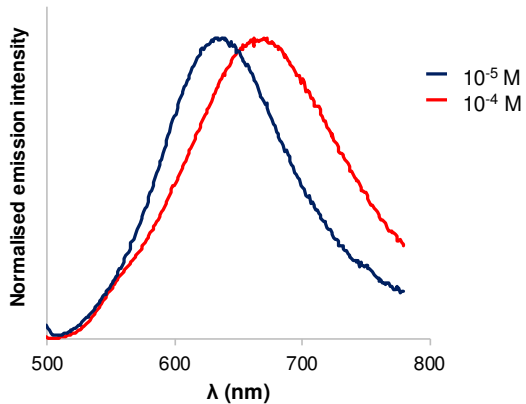


Figure S15. Emission spectra of **Pt-2** in CH_3CN at various concentrations.

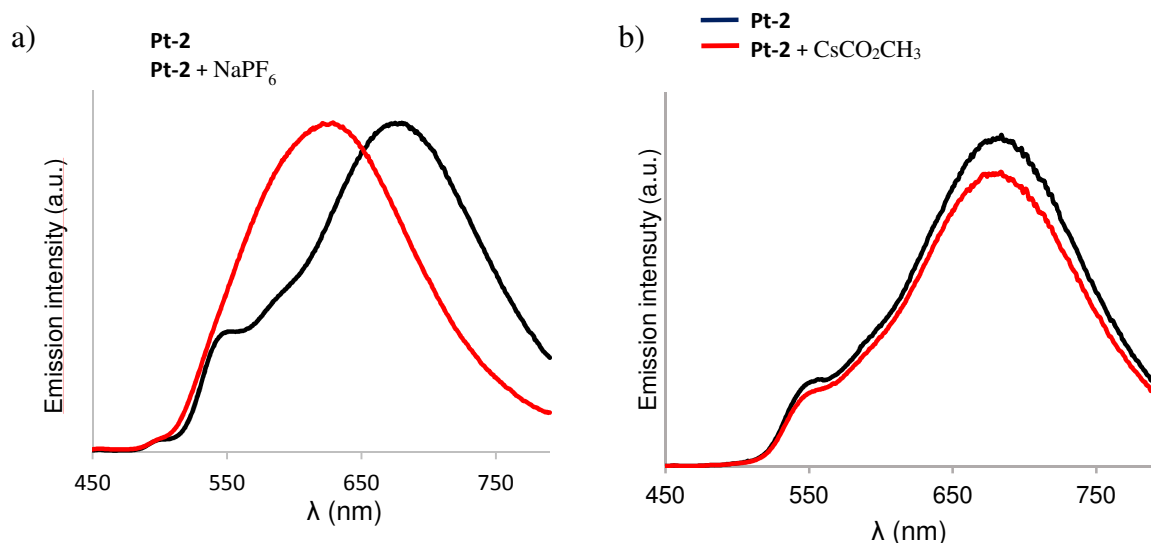


Figure S16. Emission spectra of **Pt-2** in CH_2Cl_2 ($\approx 10^{-4} \text{ M}$), before (black line) and after addition of a) 5 equiv. of NaPF_6 , b) 6 equiv. of CsCO_2CH_3 (red line).

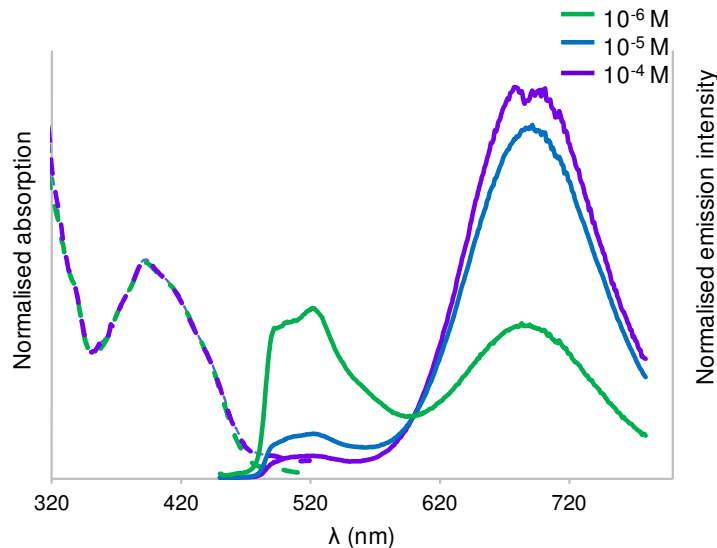


Figure S17. Absorption (dashed lines) and emission (plain lines) spectra of **Pt-3** in CH_2Cl_2 at different concentrations.

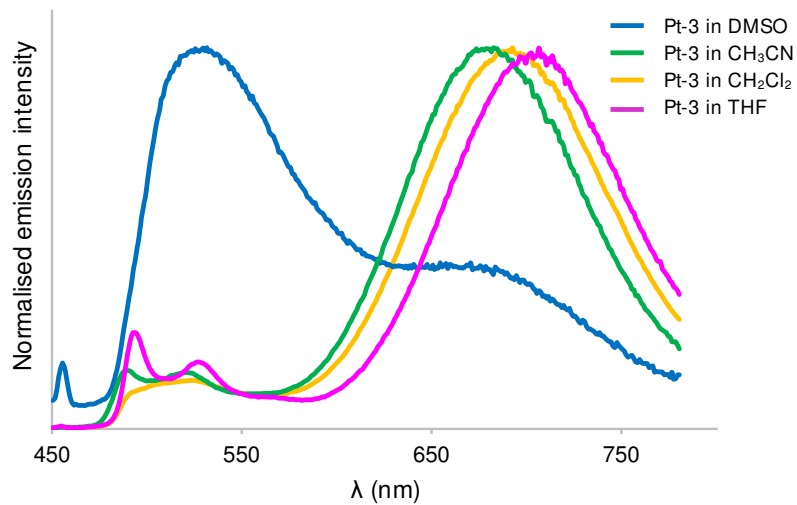


Figure S18. Emission spectra of **Pt-3** in different solvents (10^{-5}M , $\lambda_{\text{exc}} = 400\text{ nm}$).

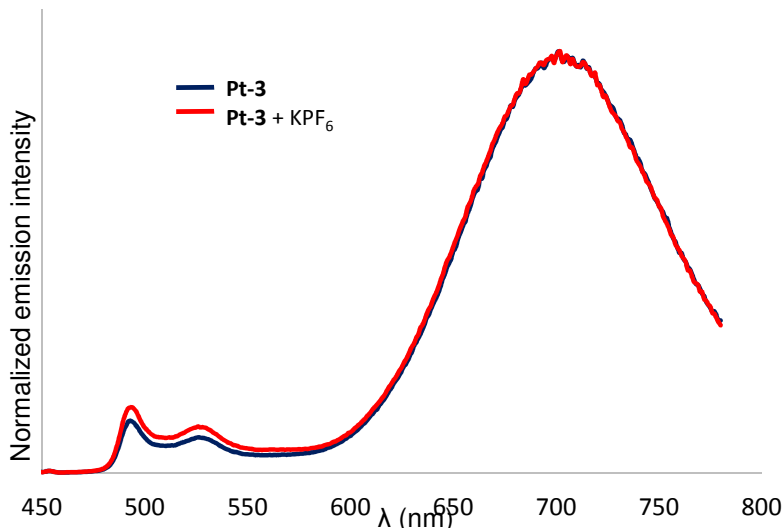


Figure S19. Emission spectra of **Pt-3** in THF (black line) and after addition of KPF₆ (6 equiv. (red line).

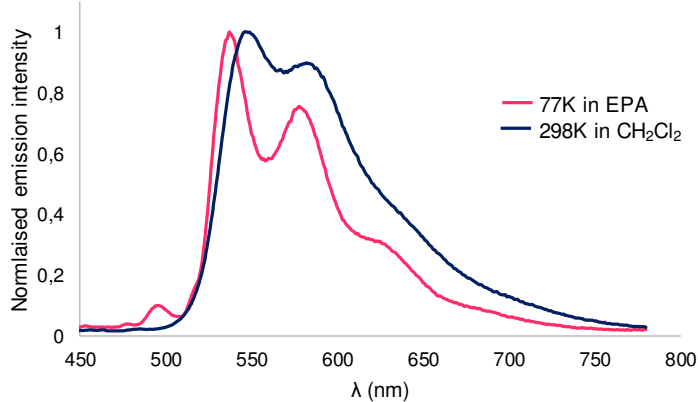


Figure S20. Emission spectra of **Pt-1** at 298K in CH₂Cl₂ (blue line) and at 77K (red line) in EPA (ethanol/isopentane/diethylether : 2/2/1) glass, $\lambda_{\text{exc}} = 400$ nm.s

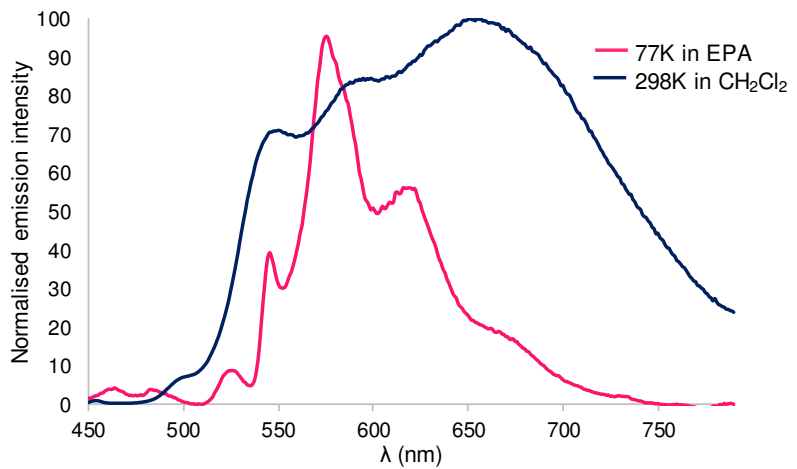


Figure S21. Emission spectra of **Pt-2** in CH_2Cl_2 at room temperature (10^{-5} M, $\lambda_{\text{exc}} = 400$ nm) and in EPA at 77K.

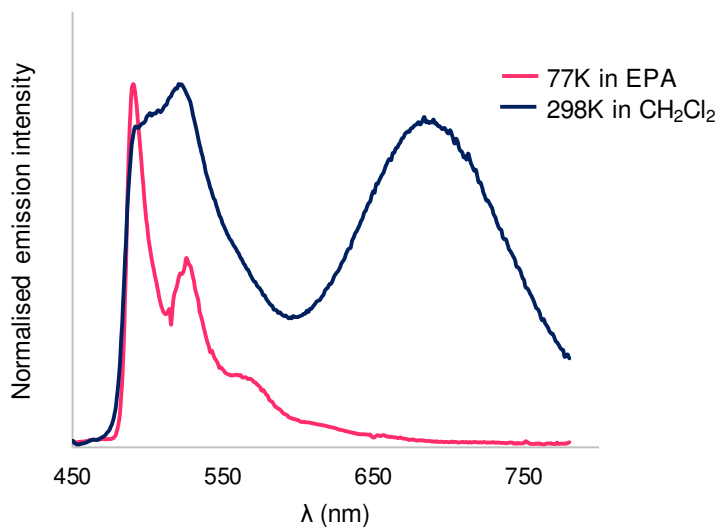


Figure S22. Emission spectra of **Pt-3** in CH_2Cl_2 at room temperature (10^{-5} M, $\lambda_{\text{exc}} = 400$ nm) and in EPA at 77K.

Table S2. Emission maxima in EPA (ethanol/isopentane/diethylether : 2/2/1) glass at 77 K, $\lambda_{\text{exc}} = 400$ nm.

Complex	$\lambda_{\text{em}}/\text{nm}$
Pt-1	538, 576, 628
Pt-2	546, 577, 620
Pt-3	491, 527, 570

Additional theoretical results

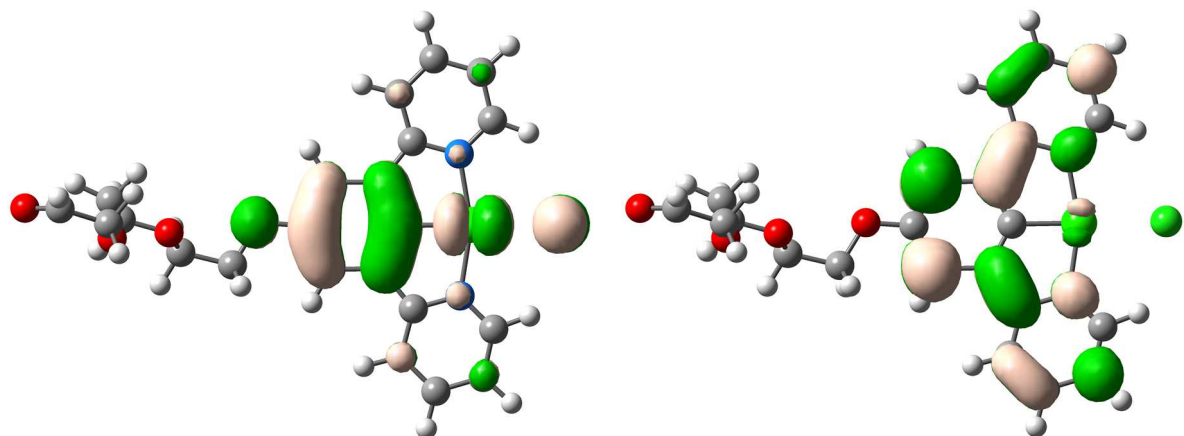


Figure S23. Representation of the HOMO (left) and LUMO (right) of **Pt-1**

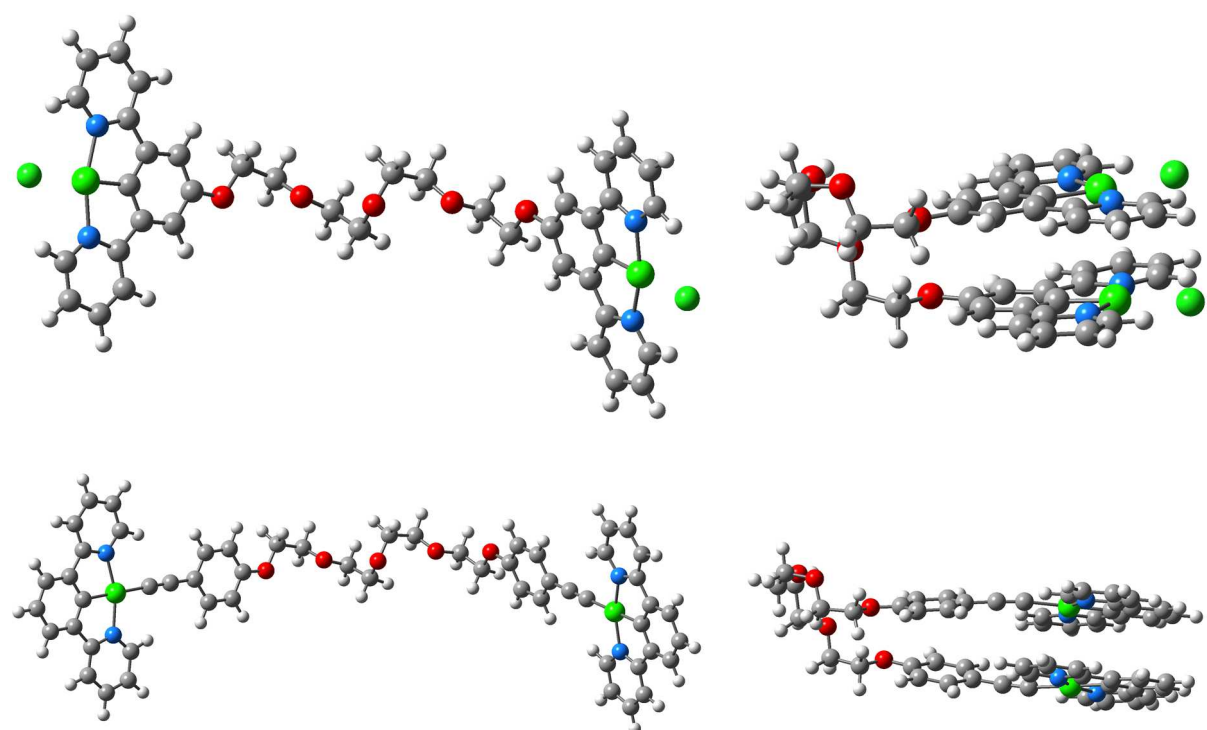


Figure S24. Representation of the DFT-optimized **Pt-2a** (top left), **Pt-2b** (top right), **Pt-3a** (bottom left), **Pt-3b** (bottom right).

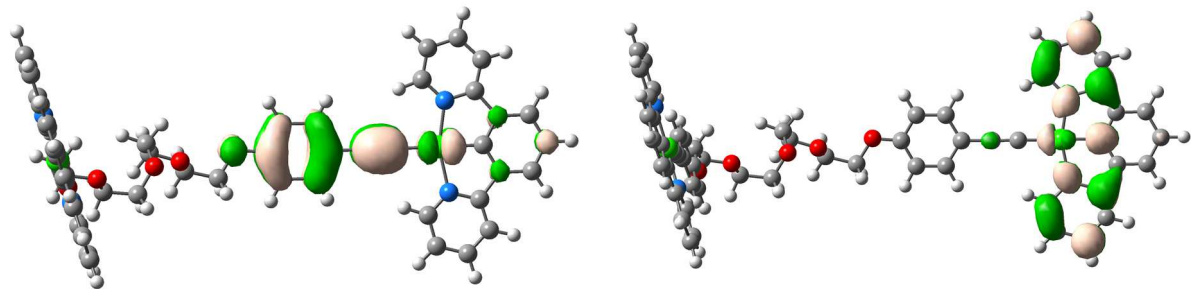


Figure S25. Representation of the HOMO (left) and LUMO (right) of **Pt-3**. Note that nearly degenerated MOs can be found on the second Pt complexes.

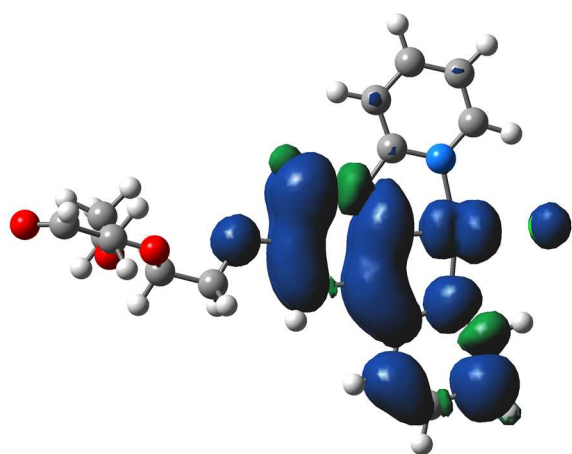


Figure S26. Representation of the spin density difference for the lowest triplet state of **Pt-1**

Table S3. TD-DFT results: transition wavelength (nm), oscillator strength and dominating MO composition (orbitals and relative weights). Only singlet excited-states showing significant oscillator strengths are described.

Complex	λ /nm	f	MO
Pt-1	420.6	0.156	H-L (0.68), H-L+1 (-0.14)
	418.3	0.013	H-L+1 (0.69), H-L (0.14)
Pt-2a	420.7	0.041	H-L+1 (0.59), H-1-L+1 (0.32), H-L+3 (-0.14)
	420.5	0.253	H-1-L (0.59), H-L+1 (-0.32), H-1-L+2 (-0.15)
	418.1	0.015	H-L+3 (0.67), H-L+1 (0.17)
	418.1	0.025	H-1-L (0.67), H-1-L (0.16)
Pt-2b	448.4	0.039	H-L (0.67), H-L+1 (-0.20)
	435.5	0.087	H-L+1 (0.63), H-L (0.20), H-L+2 (0.15), H-1-L (0.12)
	431.2	0.032	H-L+2 (0.62), H-1-L (0.24), H-L+1 (-0.17), H-1-L+1 (0.11)
	419.7	0.011	H-1-L (0.48), H-L+3 (0.34), H-1-L+1 (-0.27), H-L+2 (-0.21)
	413.4	0.019	H-2-L (0.56), H-L+2 (-0.26), H-2-L+1 (-0.22), H-1-L+2 (-0.15)
	412.2	0.010	H-1-L (0.41), H-1-L+1 (0.34), H-L+3 (-0.32), H-1-L (-0.23)
	401.7	0.016	H-2-L+1 (0.61), H-2-L (0.26), H-2-L+2 (-0.16)
	401.5	0.013	H-1-L+1 (0.52), H-L+3 (0.42), H-2-L (0.12), H-L+2 (-0.11)
	394.9	0.070	H-1-L+2 (0.65), H-L+3 (-0.15), H-2-L (0.14)
	389.2	0.001	H-2-L+3 (0.48), H-2-L+2 (-0.47), H-2-L+1 (-0.14)
	385.0	0.002	H-2-L+3 (0.47), H-2-L+2 (0.46), H-2-L+1 (0.15)
	383.4	0.008	H-1-L+3 (0.68), H-L+1 (0.13)
Pt-3a	454.8	0.200	H-L (0.60), H-1-L+1 (-0.35)
	454.4	0.151	H-1-L+1 (0.60), H-L (0.35)
	436.1	0.058	H-L+2 (0.69), H-4-L+2 (0.11)
	435.9	0.077	H-1-L+3 (0.69), H-5-L+3 (0.10)
Pt-3b	484.0	0.003	H-L (0.66), H-1-L+1 (-0.21)
	462.1	0.043	H-L+1 (0.66), H-L (0.20)
	456.3	0.203	H-1-L (0.52), H-L+2 (0.38), H-L+3 (0.22), H-1-L+1 (-0.12)
	444.1	0.001	H-L+3 (0.56), H-1-L+1 (-0.31), H-1-L (-0.22), H-1-L+1 (-0.12)
	441.3	0.001	H-L+2 (0.43), H-1-L+1 (0.41), H-1-L (-0.30), H-L+3 (0.21)
	428.4	0.000	H-1-L+1 (0.44), H-L+2 (-0.38), H-L+3 (0.27), H-1-L (0.26)
	421.2	0.008	H-1-L+3 (0.51), H-1-L+2 (0.44), H-2-L (-0.13)
	410.4	0.037	H-1-L+2 (0.52), H-1-L+3 (-0.45)
	403.2	0.055	H-2-L (0.62), H-4-L (0.18), H-3-L (0.18), H-1-L+3 (0.12)
	386.4	0.018	H-2-L+1 (0.62), H-4-L+1 (0.20), H-3-L+1 (0.19), H-2-L (0.13)

References:

- [1] G. M. Sheldrick, *Acta Cryst. A* **71**, **2015**, 3–8.
- [2] G. M. Sheldrick, *Acta Cryst. C* **71**, **2015**, 3–8.